

Trajectory Prediction for Autonomous Driving using Agent-Interaction Graph Embedding

Jilan Samiuddin*, Benoit Boulet and Di Wu

¹ **Abstract**—Trajectory prediction module in an autonomous driving system is crucial for the decision-making and safety of the autonomous agent car and its surroundings. This work presents a novel scheme called AiGem (Agent-Interaction Graph Embedding) to predict traffic vehicle trajectories around the autonomous car. AiGem tackles this problem in four steps. First, AiGem formulates the historical traffic interaction with the autonomous agent as a graph in two steps: (1) at each time step of the history frames, agent-interactions are captured using spatial edges between the agents (nodes of the graph), and then, (2) connects the spatial graphs in chronological order using temporal edges. Then, AiGem applies a depthwise graph encoder network on the spatial-temporal graph to generate graph embedding, i.e., embedding of all the nodes in the graph. Next, a sequential Gated Recurrent Unit decoder network uses the embedding of the current timestamp to get the decoded states. Finally, an output network comprising a Multilayer Perceptron is used to predict the trajectories utilizing the decoded states as its inputs. Results show that AiGem outperforms the state-of-the-art deep learning algorithms for longer prediction horizons.

Index Terms—Encoder-decoder, spatial-temporal graph, vehicle trajectory prediction

I. INTRODUCTION

Autonomous driving industry is advancing at a fast pace and demonstrating its merits to alleviate several transportation challenges with regards to safety, traffic-congestion, energy-saving, etc [1]. Despite that, deployment of autonomous cars at a mass level is still far from reality due to safety concerns. Human drivers continuously predict the maneuvers of other vehicles on the road to plan a safe and efficient future motion. Similarly, to ensure its own safety and the safety of other agents on the road, the Autonomous Driving System (ADS) must predict the motion of the surrounding agents in future with high accuracy. High accuracy in prediction will also help improve the capability of the autonomous car to infer future situations [2, 3] and consequently enhance decision-making to enrich ride quality and efficiency [4, 5].

Trajectory prediction in real-time can pose significant challenges given the dynamic and uncertain nature of roadways [6]. Although traditional prediction models such as Kalman filter [7], car-following models [8], and kinematic and dynamic models [9, 10] are hardware efficient, they become unreliable in long-term predictions when the spatial-temporal

interdependence is ignored [11]. To mitigate this concern, Ju et al. [12] combined Kalman filter, kinematic models and neural networks and obtained better performance than the traditional ones. Predicting multiple possible trajectories and ranking them based on probability distribution of the prediction model are also found in the literature [5, 13]. However, these approaches are inherently less pragmatic in real-time scenarios [6].

With significant developments in deep learning, particularly successful implementations of long-short term memory (LSTM) in capturing temporal dependencies, several works have been conducted such as [14, 15] for trajectory prediction. Despite obtaining high accuracy, these techniques do not include the interactions between the vehicles. Deo et al. [13] addresses this shortcoming by modeling the spatial interactions between the vehicles with a social tensor and then further extracting features using a convolutional social pooling techniques. However, the social tensor only preserve the spatial interaction of the last time stamp of the history, and thus, the spatial-temporal relation is not captured.

Li et al. proposes GRIP++ [16] that capture the spatial-temporal relation using fixed and dynamic homogeneous graphs. They offer two different types of edges – spatial and temporal – to capture the environmental dynamics. This is similar to what we propose, except that we use a single heterogeneous graph to feed through the graph convolutional model. Furthermore, an encoder GRU network is used in [16], whereas, in our proposed scheme, the graph convolutional model acts as the encoder network. As a result, the model size of GRIP++ is significantly larger than ours. Sheng et al. [17] also proposes a similar graph-based technique in which they stack spatial graphs from each time step in the past to form a spatial-temporal homogeneous graph. They use two different modules for extracting the spatial dependency and then extract the temporal dependency. However, since in our work, we include both the spatial and temporal aspects in the construction of the graph itself, the graph convolutional model alone is sufficient.

Lin et al. [4] uses spatial-temporal attention mechanisms with LSTM for trajectory prediction with primary focus on the explainability of their models. Katariya et al. [6] focuses on model complexity and size for faster performance and lower memory requirement. They use depthwise TCN-based (Temporal Convolutional Networks) encoder instead of LSTMs reducing the overall model size. The performances of both [4] and [6] are comparable, even though not the best, to other existing state-of-the-art methods. In our work,

¹This work was supported by Quebec's Fonds de recherche Nature et technologies (FRQNT).

The authors are with the Department of Electrical and Computer Engineering at McGill University, Montreal, QC, Canada

*Corresponding author: jilan.samiuddin@mail.mcgill.ca

we integrate attention in the depthwise graph convolutional network by graph attention networks (GAT) to capture the importance of neighboring vehicles.

This article proposes a trajectory prediction method for autonomous driving using agent-interaction graph embedding (AiGem). AiGem first constructs a heterogeneous graph from the historical data that encapsulates the interactions between the agents required for trajectory prediction of these agents. A graph encoder network then processes the graph to find embedding of the target vehicles at the current time stamp which is fed through a sequential GRU encoder network for trajectory prediction with the aid of an Multilayer Perceptron (MLP)-based output network. The results show that AiGem has higher accuracy in longer prediction horizons in contrast to the existing state-of-the-art methods with comparable accuracy for lower predictions horizons. The size of the model is much lighter than that of the compared methods except for [17].

II. PROBLEM FORMULATION

The trajectory prediction module is responsible to estimate the future positions of all the actors in the current frame based on their trajectory histories given by their global coordinates x and y with respect to the autonomous agent (also known as the ego) at the current time step, their heading θ , and the velocity v . Formally, the trajectory histories over τ_H seconds, with a sampling time t_s (i.e., over $K_H = \frac{\tau_H}{t_s} + 1$ time steps), of all the observed actors can be shown as follows

$$\mathcal{H} = [X_1, X_2, \dots, X_{K_H}] \quad (1)$$

where, $X_k = [x_k^1, y_k^1, \theta_k^1, v_k^1, \dots, x_k^{N_k}, y_k^{N_k}, \theta_k^{N_k}, v_k^{N_k}]$ with N_k being the number of actors observed at the k^{th} step. The task of the prediction module is to predict the future positions over a prediction horizon τ_F (i.e., over $K_F = \frac{\tau_F}{t_s}$ time steps) of all the N_{K_H} observed actors:

$$\mathcal{F} = [Y_{K_H+1}, Y_{K_H+2}, \dots, Y_{K_H+K_F}] \quad (2)$$

where, $Y_k = [x_k^1, y_k^1, x_k^2, y_k^2, \dots, x_k^{N_{K_H}}, y_k^{N_{K_H}}]$. Note that position with respect to the ego at the current time step K_H infers that the position of the ego ($x_{K_H}^e, y_{K_H}^e$) at present is set to (0,0) and the coordinate frame is shifted as such. This, to some extent, prevents outliers for positional features to occur during training that could lead to poor accuracy [18].

III. PRELIMINARIES

A. Graph Neural Network

Graphs are used to model the complex interactions between agents, also called the nodes, and their involvement in a neighborhood. The interactions between the nodes are presented using edges. Heterogeneous graphs, unlike homogeneous graphs, are more complex and have nodes and/or edges that can have various types or labels associated with them, indicating their different roles or semantics. For example, in our work, we use spatial and temporal edges requiring a heterogeneous graph representation. Because of the differences in type, a single edge feature tensor is unable to accommodate all edge features of the graph [19]. The computation of messages and update functions is conditioned

on node or edge type. We use PyTorch libraries in our work to operate on heterogeneous graphs which are detailed in [19].

Graph Neural Networks (GNNs) are designed for the precise task of processing graph [20]. In the node representations task, the GNN generates the matrix embedding of the nodes of size $\mathbb{R}^{n \times m}$, where, n is the number of nodes and m is the dimensionality of the features of the nodes. For node p , the GNN aggregates messages from its neighbors and then applies a neural network in several layers [21]:

$$h_p^{(i+1)} = \sigma \left(W_i \sum_{q \in \mathcal{N}(p)} \frac{h_q^{(i)}}{|\mathcal{N}(p)|} + B_i h_p^{(i)} \right), \quad (3)$$

$\forall i \in \{0, 1, \dots, L-1\}$, where, h is the embedding of a node, σ is a non-linear activation function, W_i and B_i are the weights and biases of the i^{th} layer, respectively, $\mathcal{N}(p)$ is the neighborhood of the target node p , and L is the total number of layers. Message aggregation can be done, for example, by averaging the messages from the neighbors of p .

Graph Attention Network (GAT) [22] is a GNN variant that integrates attention to focus on learning of the more relevant aspects of the input. With continual aggregation of information from the neighboring nodes q of the target node p , the network learns the importance of these neighboring nodes, also known as the attention coefficient e_{pq} . The attention coefficient is computed by applying a common linear transformation \mathbf{W} to the features (\mathbf{h}) of both p and q , followed by a shared attentional mechanism (att) as follows:

$$e_{pq} = \text{att}(\mathbf{W}\mathbf{h}_p, \mathbf{W}\mathbf{h}_q) \quad (4)$$

A single-layered feed-forward neural network is used for att in [22]. For fair comparison between the neighboring nodes, e_{pq} is normalized using the softmax function:

$$\alpha_{pq} = \frac{\exp(e_{pq})}{\sum_{k \in \mathcal{N}(p)} \exp(e_{pk})} \quad (5)$$

[22] has more detailed explanation on GAT for interested readers.

B. Gated Recurrent Unit (GRU)

GRU [23] aims to solve the vanishing gradient problem typically found in a recurrent neural network (RNN). It does so by adding an update gate u_t and a reset gate r_t which are responsible for determining the flow of information to the output. Figure 1 shows the architecture of GRU that takes the current state x_t and the previous hidden state h_{t-1} as inputs. The current output state y_t and the hidden state h_t are then obtained using the following:

$$\begin{aligned} r_t &= \sigma(W_{rx}x_t + W_{rh}h_{t-1}) \\ u_t &= \sigma(W_{ux}x_t + W_{uh}h_{t-1}) \\ \hat{h}_t &= \tanh(W_{\hat{h}x}x_t + W_{\hat{h}h}(r_t * h_{t-1})) \\ h_t &= u_t * h_{t-1} + (1 - u_t) * \hat{h}_t \\ y_t &= \sigma(W_y h_t) \end{aligned} \quad (6)$$

where, W_{rx} , W_{rh} , W_{ux} , W_{uh} , $W_{\hat{h}x}$, $W_{\hat{h}h}$, W_y are weights, and the operator $*$ is the Hadamard product. Updates are applied using equation (6) to obtain hidden states and outputs recurrently.

IV. PROPOSED METHODOLOGY

In this section, we propose a novel way to articulate the trajectory prediction problem as a sequence of connected graphs based on the historical data. Our proposed network architecture, as shown in Figure 2, illustrates the three

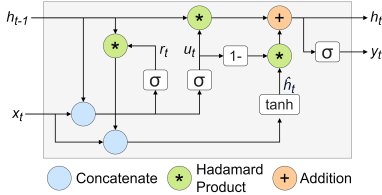


Figure 1. GRU architecture

network components forming a coherent structure for solving the trajectory prediction. The three components are (1) graph encoder network, (2) sequential GRU decoder network, and (3) output network.

A. Graph Formulation

First, the spatial graph G_k for each time step in the past, i.e., $k = 1, 2, \dots, K_H$, is generated. Figure 3(a) shows an example scenario at the k^{th} time step where the ego is surrounded by four actors of which three actors (1, 2 and 3) are in its sensing area, while the fourth actor is not in that range. Note that the sensing area in this work is defined to be a circle of radius around the ego. In the formulation of the graph as shown in Figure 3(b), alongside the ego (referred to as node e), an actor i is considered as a node of graph G if the inequality on the right-hand side of the following equation is met:

$$\mathbb{I}_{\text{node}}(i_k) = \begin{cases} 1, & \text{if } d_{ei} \leq 50 \\ 0, & \text{otherwise} \end{cases}, \quad (7)$$

where, \mathbb{I} is an indicator function and d_{ei} is the euclidean distance between the ego and the i^{th} actor. Each node $e_k, i_k \in \mathcal{N}_k$, where \mathcal{N}_k is the set of all nodes present at the k^{th} time step, has the following feature vector:

$$z_k^{e/i} = [x_k \quad y_k \quad \theta_k \quad v_k] \in \mathbb{R}^4 \quad (8)$$

The ego e always shares a bidirectional edge with a detected actor i .

$$\mathbb{I}_{\text{ea}}(E_{e_k \leftrightarrow i_k}^s) = \begin{cases} 1, & \text{if } \mathbb{I}_{\text{node}}(i_k) = 1 \\ 0, & \text{otherwise} \end{cases} \quad (9)$$

In the example shown in Figure 3, the ego and the first three actors are part of the graph with bidirectional spatial edges (i.e., d_{ei} is set as the edge feature) between the ego and the actors. Furthermore, two of the detected actors i_k and j_k share bidirectional edges between themselves if the euclidean distance d_{ij} between them is less than or equal to a predefined threshold $d_{\min} = 25$ m.

$$\mathbb{I}_{\text{aa}}(E_{i_k \leftrightarrow j_k}^s) = \begin{cases} 1, & \text{if } \mathbb{I}_{\text{node}}(i_k) = 1 \\ & \text{and } \mathbb{I}_{\text{node}}(j_k) = 1 \\ & \text{and } d_{ij} \leq d_{\min} \\ 0, & \text{otherwise} \end{cases} \quad (10)$$

In the example shown in Figure 3, while actors 1 and 2, and, 2 and 3 share an edge between themselves, actors 1 and 3 do not have an edge between them since $d_{13} > d_{\min}$. Because of these spatial edges, G_k is referred to as a spatial graph.

Next, the temporal aspect is incorporated to generate the heterogeneous graph \mathcal{G} . The temporal unidirectional edge is defined as follows:

$$\mathbb{I}_{\text{temp}}(E_{i_k \rightarrow i_{k+1}}^t) = \begin{cases} 1, & \text{if } \mathbb{I}_{\text{node}}(i_k) = 1 \\ & \text{and } \mathbb{I}_{\text{node}}(i_{k+1}) = 1, \\ 0, & \text{otherwise} \end{cases} \quad (11)$$

i.e., if actor i is within the sensing area during both the k^{th} and $(k+1)^{\text{th}}$ time frames, they are connected by a temporal unidirectional edge. Intuitively, the temporal edges encapsulate the sequential aspect of the historical data \mathcal{H} . The edge attribute is set to be the sampling time t_s . Needless to say, the temporal edge for the ego always exists between the k^{th} and $(k+1)^{\text{th}}$ time steps.

For example, as shown in the heterogeneous graph \mathcal{G} of Figure 2, from G_1 to G_2 , there exist temporal edges for actors 1 and 2 since both these actors were within the sensing area in both frames. However, actors 3 and 4 do not have the temporal edges since at $k = 2$, the former is not in the sensing area anymore while the latter materialized into the sensing area for the first time. From G_2 to G_3 , nothing changed in the sensing area, and thus, all the three actors (1, 2 and 4) have temporal edge connections. Note that the two different types of edges (spatial and temporal) in the formulation of \mathcal{G} makes it a heterogeneous graph.

B. Graph Encoder Network

The idea of the graph encoder network is to capture the context from the history \mathcal{H} presented as a spatial-temporal heterogeneous graph \mathcal{G} . The graph encoder network consists of a series of GAT convolutional networks in parallel with a series of linear layers as shown in Figure 4. The heterogeneous graph $\mathcal{G} = (Z, E)$ is forwarded to get the final encoded embedding \bar{Z}_L of all the nodes in the graph, where Z is the feature array of all nodes in \mathcal{G} and E is the edge connection array between these nodes and the corresponding edge attributes. If the total number of nodes in \mathcal{G} is N_G , then $Z \in \mathbb{R}^{N_G \times 4}$ and thus, $\bar{Z}_L \in \mathbb{R}^{N_G \times 64}$ as indicated by Figure 4. Formally, the forward pass can be defined using the following equations:

$$\begin{aligned} \bar{Z}_1 &= \text{GAT}^{(1)}(Z, E) + \text{Linear}^{(1)}(Z) \\ \bar{Z}_l &= \text{GAT}^{(l)}(\bar{Z}_{l-1}, E) + \text{Linear}^{(l)}(\bar{Z}_{l-1}), \\ &\quad \forall l = 2, \dots, L-1 \\ \bar{Z}_L &= \text{GAT}^{(L)}(\bar{Z}_{L-1}, E) + \text{Linear}^{(L)}(\bar{Z}_{L-1}) \\ &= [\bar{G}_1 \quad \bar{G}_2 \quad \dots \quad \bar{G}_{K_H}] \end{aligned} \quad (12)$$

where, \bar{G}_k contains the node embedding of the nodes of the spatial graph G_k . In the above discussed example, $\bar{Z}_L \in \mathbb{R}^{12 \times 64}$ and $\bar{G}_1, \bar{G}_2, \bar{G}_3 \in \mathbb{R}^{4 \times 64}$. However, we are only interested in the embedding $\bar{G}_{K_H} \in \bar{Z}_L$ – this fixed-size representation contains meaningful features about the entire input sequence due to the unidirectional temporal edges.

C. Sequential GRU Decoder Network

The task is to predict the trajectory of actor $i_{K_H} \in \mathcal{N}_{K_H}$. Without any loss of generality, for simplicity, we will refer to actor i_{K_H} as i . The task of the decoder is to generate a decoded state based on the current hidden state and the previously generated decoded state. Needless to say, at the beginning, the sequential GRU decoder network takes as inputs the initial hidden states $h_{K_H}^i$ (initialized as zeros) and

$$\bar{z}_{K_H}^i = f(\bar{G}_{K_H}, i) \in \bar{G}_{K_H} \quad (13)$$

where, $f(\bar{G}_{K_H}, i)$ is a function that extracts the corresponding embedding of actor i from \bar{G}_{K_H} . We also apply a residual connection similar to [24] to the output g of the GRU as it

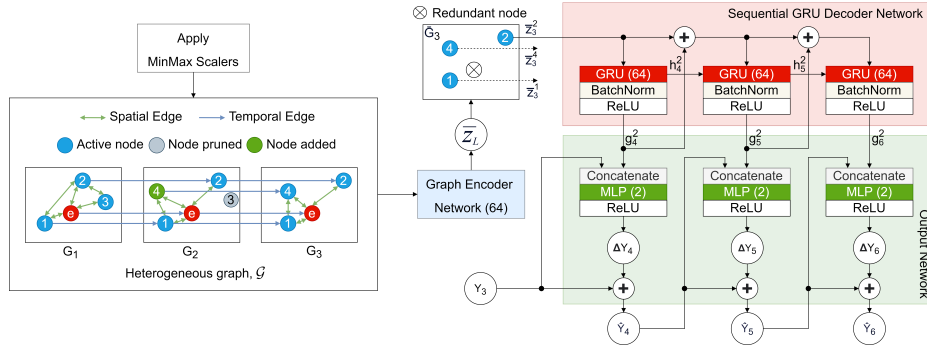


Figure 2. Proposed network architecture AiGem with $K_H = 3$ (number of steps in the history including the present), $K_F = 3$ (number of steps to predict). Modules (GRUs and MLPs) inside the networks with the same color share the same weights. The number within parenthesis represents the output dimension of the module.

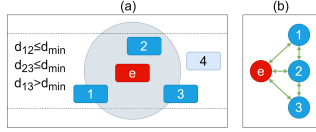


Figure 3. (a) An example scenario of an ego (in red) surrounded by actors (blue) of which actors 1, 2, and 3 are in its sensing area (gray circle), and, (b) Graph formulation with ego connected to the sensed actors via bidirectional spatial edges.

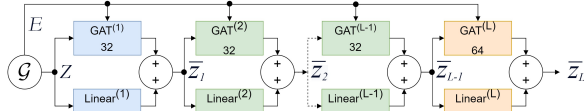


Figure 4. Graph encoder network with L number of layers. GAT modules with the same color share same weights and linear modules with the same color share same weights.

allows to leverage previously learned representations. Thus, the forward pass in the network can be defined as follows:

$$\begin{aligned} (g_{K_H+1}^i, h_{K_H+1}^i) &= \text{GRU}(\bar{z}_{K_H}^i, h_{K_H}^i) \\ (g_{K_H+2}^i, h_{K_H+2}^i) &= \text{GRU}(\bar{z}_{K_H}^i + g_{K_H+1}^i, h_{K_H+1}^i) \\ (g_k^i, h_k^i) &= \text{GRU}(g_{k-1}^i + g_{k-2}^i, h_{k-1}^i), \\ &\quad \text{for } k = K_H + 3, \dots, K_H + K_F \end{aligned} \quad (14)$$

D. Output Network

For the prediction horizon $k = K_H + 1, \dots, K_H + K_F$, the output network consists of a Multilayer perceptron (MLP) that takes g_k^i as input to predict the trajectory of actor i . The output of the MLP ΔY_k^i is the change in position in both the x and y coordinates with respect to the previous actual or the estimated position. Thus, the final predicted position \hat{Y}_k^i for the prediction horizon is obtained as follows:

$$\begin{aligned} \hat{Y}_{K_H+1}^i &= \text{MLP}(C(g_{K_H+1}^i, Y_{K_H}^i)) + Y_{K_H}^i \\ \hat{Y}_k^i &= \text{MLP}(C(g_k^i, \hat{Y}_{k-1}^i)) + \hat{Y}_{k-1}^i, \\ &\quad \text{for } k = K_H + 2, \dots, K_H + K_F \end{aligned} \quad (15)$$

where, $Y_{K_H}^i$ is the current position of actor i and C is a concatenation function. Note that AiGem does not simultaneously predict trajectories of the N_{K_H} actors, rather predicts trajectories of each actor at a time.

V. EXPERIMENT SETUP AND RESULTS

A. Datasets

NGSIM datasets [25, 26], collected by the Federal Highway Administration of the U.S. Department of Transportation, are used to evaluate the performance of our proposed model. In this work, we use the datasets for highways US-101 [26] and I-80 [25]. The NGSIM datasets consist of 45 minutes of vehicle trajectories transcribed from videos – these videos are obtained through synchronized cameras mounted on top of adjacent buildings of the highway of interest. Many deep-learning techniques [4, 6, 13, 16, 17, 27] use these two datasets for performance assessment.

B. Data Processing

The data in NGSIM were recorded at 10 frames per second, i.e., the sampling time is 0.1 second. However, to make a fair comparison with other techniques [4, 6, 13, 16, 17] which downsampled the data to 0.2 second, we do the same as well. The trajectories are then segmented into 8 seconds blocks so that the first 3 seconds can be used as historical observation, and the remaining 5 seconds can be used as prediction ground truth. Similar to [4, 6], we split our dataset into 70% training data, 10% validation data, and 20% test data. Note that in the NGSIM datasets, the heading values θ of the vehicles are not provided. However, given the history of a vehicle's trajectory, we can easily calculate θ for this past trajectory using basic trigonometry.

MinMax normalization is applied to all the inputs. The range for scaling the positions and the heading is $(-1, 1)$ and the range for scaling the velocity and the distance between the vehicles (spatial edge) is $(0, 1)$. However, scaling is not applied on the temporal edges since the magnitude of the sampling time (0.2 second) is already within the range $(0, 1)$.

C. Baselines

Recently, several deep-learning techniques have applied to conduct the task of trajectory prediction on the NGSIM data. We use the following models for comparing the performance of our proposed AiGem:

(1) **CS-LSTM** [13]: It utilizes an LSTM encoder-decoder model with a social pooling layer for feature extraction.

(2) **GRIP++** [16]: It utilizes a LSTM encoder-decoder model with fixed and dynamic graphs to capture the environmental dynamics.

(3) **STA-LSTM** [4]: It combines spatial-temporal attention with LSTM and increases the interpretability of the predictions.

(4) **DeepTrack** [6]: It provides a light-weight prediction model by introducing temporal and depthwise convolutions for capturing vehicle dynamics.

(5) **GSTCN** [17]: It utilizes a graph-based spatial-temporal convolutional network to first learn the spatial features and then extract the temporal features. Finally, GRU is used for prediction using the extracted features.

D. Evaluation Metrics

Our proposed model, AiGem, is compared against existing deep-learning techniques using different metrics. The followings are commonly used as a measure of prediction accuracy and performance of the system:

Average displacement error (ADE): It is the average euclidean distance between the predicted positions \hat{Y}_k and the ground truth Y_k for $k = K_H + 1, \dots, K_H + K_F$ and for N_{K_H} actors:

$$\text{ADE} = \frac{\sum_{n=1}^{N_{K_H}} \sum_{k=K_H+1}^{K_H+K_F} \|\hat{Y}_k^i - Y_k^i\|_2}{K_F N_{K_H}} \quad (16)$$

Final displacement error (FDE): It is the average euclidean distance between \hat{Y}_k and Y_k for the last predicted step $k = K_H + K_F$ and for N_{K_H} actors:

$$\text{FDE} = \frac{\sum_{n=1}^{N_{K_H}} \|\hat{Y}_{K_H+K_F}^i - Y_{K_H+K_F}^i\|_2}{N_{K_H}} \quad (17)$$

Root mean square error (RMSE): It is the square root of the mean squared error between \hat{Y}_k and Y_k at k^{th} step for N_{K_H} actors:

$$\text{RMSE} = \sqrt{\frac{1}{N_{K_H}} \sum_{n=1}^{N_{K_H}} (\hat{Y}_k^i - Y_k^i)^2} \quad (18)$$

We also compare the model size (i.e., number of parameters in the model) of AiGem with the baselines.

E. Ablation Study

We conduct two ablation studies, particularly, (1) the effect of d_{\min} as described in equation (10), and, (2) the effect of concatenation at the MLP input defined in equation (15) on the performance of the AiGem.

(1) For the formulation of the graph in section IV-A, equation (10) defines that there exists a bidirectional edge between two actors if the distance between them is less than a predefined threshold d_{\min} . We set the values of d_{\min} to different values and compare the performance of AiGem for these different values. Figure 5 shows how our proposed model performs for different values of d_{\min} . It is clear that when $d_{\min} = 0$ m (i.e., none of the detected actors are connected with each other using an edge in the spatial graph), the error is maximum for all the prediction horizons.

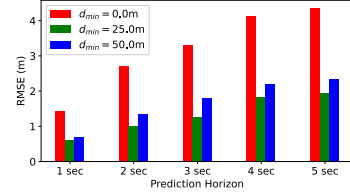


Figure 5. Comparison of performance of AiGem for different values of d_{\min}

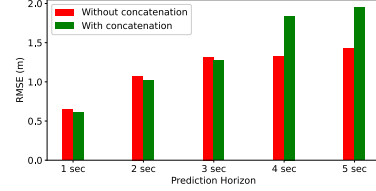


Figure 6. Comparison of performance of AiGem with and without concatenation of the output

Therefore, connecting actors using edges in the spatial graph indeed help minimizing the loss. Next, it can be observed that the error also increases when d_{\min} is increased from 25 m to 50 m, i.e., the number of bidirectional edges between actors increases due to increase in d_{\min} . This phenomenon makes intuitive sense since in real-life scenarios, a human driver is more likely to make decisions based on nearer actors than actors that are further. Since $d_{\min} = 25$ m results in the minimum RMSE value, we use that in the formulation of the spatial graphs.

(2) In the proposed architecture, as defined in equation (15), we concatenate the output with the decoded embedding at the input of the MLP of the output network. We want to see the performance without concatenation, i.e., modify equation (15) to:

$$\begin{aligned} \hat{Y}_{K_H+1}^i &= \text{MLP}(g_{K_H+1}^i) + Y_{K_H}^i \\ \hat{Y}_k^i &= \text{MLP}(g_k^i) + \hat{Y}_{k-1}^i, \\ &\text{for } k = K_H + 2, \dots, K_H + K_F \end{aligned} \quad (19)$$

Figure 6 shows the differences between the performances with and without concatenation for different prediction horizons. It is clear that for lower prediction horizons (1, 2 and 3 seconds), concatenation has clear advantage. However, for longer predictions (4 and 5 seconds), concatenation degrades the performance. Since concatenation has advantage over three prediction horizons out of five, we use the concatenation approach to report in the remaining article.

F. AiGem Training

In our work, we used the Adam optimizer to optimize AiGem with a learning rate of 0.001. To mitigate overfitting of the network and improve generalization performance of our proposed network, dropout regularization technique is applied during training, i.e., a dropout rate of 5% was applied. We train a separate model for each target horizon. Figure 7 shows the training evolution of the AiGem models for different prediction horizons. Note that it took approximately 100 training epochs to get the best model for each prediction horizon – the best model refers to the model with the lowest validation loss. As the prediction horizon increases, overfitting becomes evident in the training of AiGem.

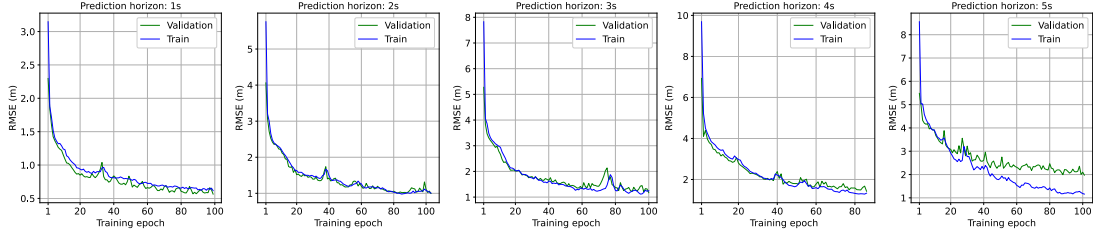


Figure 7. Training of separate AiGem models for different prediction horizons showing RMSE evolution for training and validation datasets

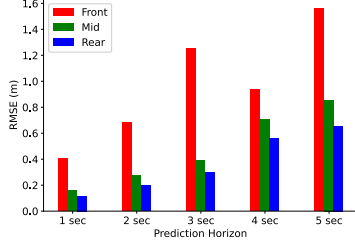


Figure 8. Performance assessment of AiGem for predicting trajectories of actors based on the positions around the ego

G. Results

Table I shows the performance comparison between AiGem and other baselines. In RMSE comparison, AiGem achieves comparable results in short predictions, i.e., the first two seconds. However, in the longer prediction horizons, it is at the forefront of all the models. For 3 seconds and 4 seconds prediction, it achieves a lead of 4.5% and 8.5% from the second best, respectively. The lead becomes significant for 5 seconds – 33.7% improvement from the second best. This shows that AiGem is more proficient in extracting useful features for longer predictions.

As shown in Table I, compared to CS-LSTM, GRIP++, STA-LSTM, DeepTrack and GSTCN, AiGem reduces ADE by 38.0%, 11.8%, 24.8%, 29.4% and 6.6%, respectively. For the metric FDE, AiGem has the best score among all the models. It outperforms the baselines by 23.1%, 18.7% and 20.9% compared to CS-LSTM, STA-LSTM and DeepTrack, respectively.

The AiGem is also the second lightest model in terms of model size as shown in Table I. Compared to heaviest model GRIP++, it has 85.5% less number of parameters. The lightest model is the GSTCN with 33.2% less parameters than ours. The smaller size of GSTCN is likely due to restricting the graph to two laterally adjacent lanes and ± 100 meters of the roadways [27] in contrary to AiGem. As explained earlier in section II, the shifting of the coordinate frame with respect to the current position of the ego allows our model to adjust easily to any section of the road.

In summary, our proposed model AiGem is lightweight yet excels in forecasting trajectories over longer prediction horizons, outperforming baseline models in both longer horizon predictions, the ADE score and the FDE score.

Furthermore, we analyze the performance of AiGem on predicting trajectories of actors based on their positions around the ego. To do that, we broadly define three positions:

Table I
PREDICTION METRICS AND MODEL SIZE COMPARISON OF AiGEM WITH THE BASELINES. THE BEST RESULTS ARE IN BOLD AND THE SECOND BEST ARE UNDERLINED.

Model	ADE (m)	FDE (m)	RMSE (m)					Params (K)
			1s	2s	3s	4s	5s	
CS-LSTM	2.29	3.34	0.61	1.27	2.09	3.10	4.37	192
GRIP++	1.61	–	<u>0.38</u>	<u>0.89</u>	1.45	2.14	<u>2.94</u>	496*
STA-LSTM	1.89	<u>3.16</u>	0.37	0.98	1.71	2.63	3.78	125
DeepTrack	2.01	3.25	0.47	1.08	1.83	2.75	3.89	109
GSTCN	<u>1.52</u>	–	0.44	0.83	<u>1.33</u>	<u>2.01</u>	2.98	49.8
AiGem (Ours)	1.42	2.57	0.61	1.02	1.27	1.84	1.95	<u>74.5</u>

*[16] does not report the number of parameters but we extracted this number from their shared code [28]

- 1) **Front position:** If an actor is more than 15 m ahead longitudinally from the ego, it is considered in the front position.
- 2) **Rear position:** If an actor is more than 15 m behind longitudinally from the ego, it is considered in the rear position.
- 3) **Mid position:** If an actor is between ± 15 m longitudinally of the ego, it is considered in the mid position.

Figure 8 shows the performance of AiGem in predicting trajectories of actors based on the positions described above. It can be clearly observed that our proposed model is able to predict trajectories of actors more accurately that are in rear position with respect to the ego, in contrast to the mid and front positions, for all prediction horizons. The model achieves the least accuracy when the actors are in the front position. Thus, it can be concluded, when AiGem predicts the trajectory of an actor i with respect to the ego, it considers front actors relative to i to have more impact on its future decision-making. On the other hand, rear actors relative to i has lesser impact on its future decision-making. It is important to note that the graph formulation is constrained by the sensing area of the ego – this implies that the actors positioned in the rear with respect to the ego observes actors in front of them while the actors positioned in the front with respect to the ego observes actors behind them.

VI. CONCLUSION

In this article, we propose a deep learning model called the AiGem that constructs a heterogeneous graph from the historical data using spatial and temporal edges to capture interactions between the agents. A graph encoder network generates embedding for the target actors in the current timestamp which is fed through a sequential GRU decoder network. The decoded states from the decoder network are then utilized to predict future trajectories using an MLP in the output network. NGSIM datasets have been used for performance assessment. The results show that AiGem achieves comparable accuracy to state-of-the-art prediction algorithms for shorter prediction horizons. For longer prediction horizons, particularly 3, 4 and 5 seconds, it outperforms all the baselines used. The size of the model is better than most of them and comparable to the lightest.

REFERENCES

- [1] Y. Huang, J. Du, Z. Yang, Z. Zhou, L. Zhang, and H. Chen, "A survey on trajectory-prediction methods for autonomous driving," *IEEE Transactions on Intelligent Vehicles*, vol. 7, no. 3, pp. 652–674, 2022.
- [2] X. Li, Z. Sun, D. Cao, Z. He, and Q. Zhu, "Real-time trajectory planning for autonomous urban driving: Framework, algorithms, and verifications," *IEEE/ASME Transactions on mechatronics*, vol. 21, no. 2, pp. 740–753, 2015.
- [3] S. Bae, D. Saxena, A. Nakhaei, C. Choi, K. Fujimura, and S. Moura, "Cooperation-aware lane change maneuver in dense traffic based on model predictive control with recurrent neural network," in *2020 American Control Conference (ACC)*. IEEE, 2020, pp. 1209–1216.
- [4] L. Lin, W. Li, H. Bi, and L. Qin, "Vehicle trajectory prediction using lstms with spatial-temporal attention mechanisms," *IEEE Intelligent Transportation Systems Magazine*, vol. 14, no. 2, pp. 197–208, 2021.
- [5] T. Phan-Minh, E. C. Grigore, F. A. Boulton, O. Beijbom, and E. M. Wolff, "Covnet: Multimodal behavior prediction using trajectory sets," in *Proceedings of the IEEE/CVF conference on computer vision and pattern recognition*, 2020, pp. 14 074–14 083.
- [6] V. Katariya, M. Baharani, N. Morris, O. Shoghli, and H. Tabkhi, "Deeptrack: Lightweight deep learning for vehicle trajectory prediction in highways," *IEEE Transactions on Intelligent Transportation Systems*, vol. 23, no. 10, pp. 18 927–18 936, 2022.
- [7] B. Mourlillon, D. Gruyer, A. Lambert, and S. Glaser, "Kalman filters predictive steps comparison for vehicle localization," in *2005 IEEE/RSJ International Conference on Intelligent Robots and Systems*. IEEE, 2005, pp. 565–571.
- [8] Z. Sheng, S. Xue, Y. Xu, and D. Li, "Real-time queue length estimation with trajectory reconstruction using surveillance data," in *2020 16th International Conference on Control, Automation, Robotics and Vision (ICARCV)*. IEEE, 2020, pp. 124–129.
- [9] A. Polychronopoulos, M. Tsogas, A. J. Amditis, and L. Andreone, "Sensor fusion for predicting vehicles' path for collision avoidance systems," *IEEE Transactions on Intelligent Transportation Systems*, vol. 8, no. 3, pp. 549–562, 2007.
- [10] M. Brännström, E. Coelingh, and J. Sjöberg, "Model-based threat assessment for avoiding arbitrary vehicle collisions," *IEEE Transactions on Intelligent Transportation Systems*, vol. 11, no. 3, pp. 658–669, 2010.
- [11] S. Lefèvre, D. Vasquez, and C. Laugier, "A survey on motion prediction and risk assessment for intelligent vehicles," *ROBOMECH journal*, vol. 1, pp. 1–14, 2014.
- [12] C. Ju, Z. Wang, C. Long, X. Zhang, and D. E. Chang, "Interaction-aware kalman neural networks for trajectory prediction," in *2020 IEEE Intelligent Vehicles Symposium (IV)*. IEEE, 2020, pp. 1793–1800.
- [13] N. Deo and M. M. Trivedi, "Convolutional social pooling for vehicle trajectory prediction," in *Proceedings of the IEEE conference on computer vision and pattern recognition workshops*, 2018, pp. 1468–1476.
- [14] A. Zyner, S. Worrall, and E. Nebot, "A recurrent neural network solution for predicting driver intention at unsignalized intersections," *IEEE Robotics and Automation Letters*, vol. 3, no. 3, pp. 1759–1764, 2018.
- [15] L. Xin, P. Wang, C.-Y. Chan, J. Chen, S. E. Li, and B. Cheng, "Intention-aware long horizon trajectory prediction of surrounding vehicles using dual lstm networks," in *2018 21st International Conference on Intelligent Transportation Systems (ITSC)*. IEEE, 2018, pp. 1441–1446.
- [16] X. Li, X. Ying, and M. C. Chuah, "Grip++: Enhanced graph-based interaction-aware trajectory prediction for autonomous driving," *arXiv preprint arXiv:1907.07792*, 2019.
- [17] Z. Sheng, Y. Xu, S. Xue, and D. Li, "Graph-based spatial-temporal convolutional network for vehicle trajectory prediction in autonomous driving," *IEEE Transactions on Intelligent Transportation Systems*, vol. 23, no. 10, pp. 17 654–17 665, 2022.
- [18] A. Khamis, Z. Ismail, K. Haron, and A. T. Mohamm, "The effects of outliers data on neural network performance," *Journal of Applied Sciences*, vol. 5, no. 8, pp. 1394–1398, 2005.
- [19] PyTorch Geometric, "Heterogeneous graph learning," [Online]. Available: <https://pytorch-geometric.readthedocs.io/en/latest/notes/heterogeneous.html>, Last Accessed: April 2024.
- [20] F. Scarselli, M. Gori, A. C. Tsoi, M. Hagenbuchner, and G. Monfardini, "The graph neural network model," *IEEE transactions on neural networks*, vol. 20, no. 1, pp. 61–80, 2008.
- [21] J. Leskovec, "CS224W: Machine learning with Graphs, Stanford University," [Online]. Available: <http://web.stanford.edu/class/cs224w/>, Last Accessed: July 2023.
- [22] P. Veličković, G. Cucurull, A. Casanova, A. Romero, P. Lio, and Y. Bengio, "Graph attention networks," *arXiv preprint arXiv:1710.10903*, 2017.
- [23] K. Cho, B. Van Merriënboer, C. Gulcehre, D. Bahdanau, F. Bougares, H. Schwenk, and Y. Bengio, "Learning phrase representations using rnn encoder-decoder for statistical machine translation," *arXiv preprint arXiv:1406.1078*, 2014.
- [24] K. He, X. Zhang, S. Ren, and J. Sun, "Deep residual learning for image recognition," in *Proceedings of the IEEE conference on computer vision and pattern recognition*, 2016, pp. 770–778.
- [25] J. Colyar and J. Halkias, "Next generation simulation (ngsim), interstate 80 freeway dataset," *Federal Highway Administration, Tech. Rep.*, 2006.
- [26] —, "Next generation simulation (ngsim), us highway-101 dataset," *Federal Highway Administration, Tech. Rep.*, 2007.
- [27] G. Alinezhad Noghre, V. Katariya, A. Danesh Pazho, C. Neff, and H. Tabkhi, "Pishgu: Universal path prediction network architecture for real-time cyber-physical edge systems," in *Proceedings of the ACM/IEEE 14th International Conference on Cyber-Physical Systems (with CPS-IoT Week 2023)*, 2023, pp. 88–97.
- [28] X. Li, X. Ying, and M. C. Chuah, "Grip," <https://github.com/xincoder/GRIP>, 2019.